Supporting Information for:

Magnetic Reconstruction at Grain Boundaries in Ni-dihalides

Min Yang[1], Baishun Yang[2], Yuheng Liu[1], Daniel Hernangómez-Pérez[2], Yu Yan[1*]*

[1] Key Laboratory of Physics and Technology for Advanced Batteries (Ministry of Education), Department of Physics, Jilin University, Changchun, 130012, China

[2] CIC nanoGUNE BRTA, Tolosa Hiribidea 76, 20018 San Sebastián, Spain

[*]Corresponding Authors: b.yang@nanogune.eu
[*]Corresponding Authors: yanyu@jlu.edu.cn

COMPUTATIONAL METHODS

First-principles calculations were performed using the Vienna Ab initio Simulation Package (VASP) based on density functional theory (DFT).[1] The Perdew-Burke-Ernzerhof (PBE) functional was employed for the exchange-correlation potential.[2] To account for the strong electron correlations at the Ni-*d* orbitals, the DFT+U method was used, with an effective Hubbard parameter U = 1.8 eV and J = 0.8 eV.[3,4] For monolayer NiX_2 (X = Cl, Br and I), a plane-wave cutoff energy of 500 eV was used, and Brillouin zone integration was performed using a 19×19×1 Γ-centered *k*-point mesh. For the Σ7 GB system, the cutoff energy was reduced to 400 eV with a 4×1×1 k-point mesh. A vacuum layer of 25 Å was considered along the *z*-direction for all systems to eliminate spurious periodic interactions. Calculations were considered converged for the NiX_2 monolayers when forces on atoms were less than 0.001 eV/Å and total energies below 10^{-6} eV between consecutive SCF cycles. These criteria were set to 0.01 eV/Å and 10^{-5} eV for the GB system. The optimized lattice constant for monolayer $NiCl_2$ was 3.49 Å, showing excellent agreement with previously reported values.[3] Ab initio molecular dynamic simulations (AIMD) at 300 K were performed within a 2 × 1× 1 CSL supercell and a 2 × 1 × 1 *k*-point grid. For the AIMD simulations, the canonical ensemble method[5] was adopted and the simulation time limited to 5.0 ps, with a time step of 1 fs. The Nosé-Hoover method[6] is applied to control the temperature at 300 K. All magnetic exchange parameters reported in this work were calculated using the four-state energy mapping method.[7,8]

Atomistic spin simulations were performed using the VAMPIRE package.[9] In-plane periodic boundary conditions were considered. In the simulations, the field-cooling method was implemented by using a randomized initial spin configuration. The temperature was reduced from 50 K to 1 K in 1 K steps, then cooled to approach 0 K. Each simulation ran for 3×10^6 Monte Carlo steps per site. Spin scalar chirality Ω_i was calculated according to[10]:

$$\tan\left(\frac{\Omega_i}{2}\right) = \frac{\mathbf{S_1}\cdot(\mathbf{S_2}\times\mathbf{S_3})}{1+\mathbf{S_1}\cdot\mathbf{S_2}+\mathbf{S_2}\cdot\mathbf{S_3}+\mathbf{S_3}\cdot\mathbf{S_1}}$$

where Ω_i is calculated for each triangular plaquette defined by spins $\mathbf{S_1}$, $\mathbf{S_2}$, and $\mathbf{S_3}$.

The topological charge Q for a selected skyrmion/antiskyrmion is calculated by integral the spin scalar chirality in the skyrmion diameter.

$$Q = \frac{1}{4\pi}\sum_i \Omega_i$$

The calculated topological charge for the skyrmion and antiskyrmion in Σ7 NiCl2 at B_z=2.5T is Q= -0.87 and 0.83, respectively. Such non-integer topological charge is a result of the non-uniform skyrmion boundary which shows spin helical textures.

Table S1. Exchange coupling tensors for first-nearest neighbor (J_1), second-nearest neighbor (J_2), third-nearest neighbor (J_3), and single-ion anisotropy (SIA) in monolayer $NiCl_2$. All the units are in meV.

$NiCl_2$	J_{xx}	J_{yy}	J_{zz}	J_{xy}	J_{yx}	J_{xz}	J_{zx}	J_{yz}	J_{zy}	SIA
J_1	-5.61	-5.62	-5.62	0.00	0.00	0.00	0.00	0.00	0.00	
J_2	-0.06	-0.06	-0.06	0.00	0.00	0.00	0.00	0.00	0.00	0.00
J_3	1.83	1.82	1.82	0.00	0.00	0.00	0.00	0.00	0.00	

Table S2. Exchange coupling tensors for Σ7 $NiCl_2$. All the units are in meV. The subscript in the exchange parameter J denotes the index of the Ni-Ni pairs at the Σ7 $NiCl_2$ (see **Figure S1a** for atomic index).

Σ7 $NiCl_2$	J_{xx}	J_{yy}	J_{zz}	J_{xy}	J_{yx}	J_{xz}	J_{zx}	J_{yz}	J_{zy}
$J_{0\text{-}15}$	5.81	5.95	4.90	0.82	-0.54	-0.87	1.11	0.44	-0.32
$J_{0\text{-}17}$	-3.36	-3.88	-2.47	-0.71	-0.06	-0.05	0.05	-0.13	0.13
$J_{16\text{-}0}$	-6.28	-6.61	-6.10	-0.05	-1.60	-0.71	-0.85	-0.03	-0.07
$J_{1\text{-}15}$	27.18	26.86	27.70	-0.29	0.38	0.40	-0.46	-0.01	-0.01
$J_{2\text{-}16}$	-0.20	-0.50	-0.17	-3.80	0.68	-0.03	-0.03	-0.02	-0.01
$J_{15\text{-}16}$	-2.40	-2.74	-2.00	0.05	-0.10	-0.26	0.10	0.03	-0.12
$J_{15\text{-}17}$	-6.70	-6.38	-5.69	-0.02	-0.11	0.00	-0.23	0.10	-0.07
$J_{15\text{-}18}$	-1.53	-1.93	-1.45	0.07	-0.16	-0.04	-0.07	-0.17	0.16
$J_{16\text{-}18}$	-2.42	-3.78	-3.10	0.00	0.36	-0.05	0.23	-0.59	0.19
$J_{17\text{-}18}$	-4.15	-6.07	-4.80	-1.06	0.05	-0.13	0.04	0.00	0.00

Table S3. Exchange coupling tensors for Σ7 $NiBr_2$. All the units are in meV.

Σ7 $NiBr_2$	J_{xx}	J_{yy}	J_{zz}	J_{xy}	J_{yx}	J_{xz}	J_{zx}	J_{yz}	J_{zy}
$J_{0\text{-}15}$	10.10	10.12	10.13	0.83	-0.68	-0.49	0.60	0.85	-0.68
$J_{0\text{-}17}$	-2.14	-2.35	-2.26	0.39	-0.33	-0.21	-1.15	-0.26	0.14
$J_{16\text{-}0}$	-6.81	-7.09	-7.03	-0.32	0.06	0.43	0.07	-0.46	1.21
$J_{1\text{-}15}$	15.07	15.13	15.24	-1.52	1.52	0.41	-0.01	0.24	0.14
$J_{2\text{-}16}$	-0.23	-0.36	-0.29	-0.04	0.04	0.10	0.11	-0.04	-0.15
$J_{15\text{-}16}$	-3.66	-3.50	-3.60	-0.47	0.52	0.09	-0.03	0.24	0.14
$J_{15\text{-}17}$	-7.52	-7.43	-7.43	0.35	-0.63	0.54	-1.19	0.17	-0.44
$J_{15\text{-}18}$	-2.79	-3.17	-2.92	0.02	0.09	0.05	-1.42	0.00	-0.59
$J_{16\text{-}18}$	-1.20	-1.32	-1.26	-0.05	-0.15	0.23	-0.06	-0.35	-0.13
$J_{17\text{-}18}$	-5.54	-5.19	-5.19	0.12	0.02	0.14	-0.09	0.10	0.13

Table S4. Exchange coupling tensors for Σ7 NiI_2 GB. All the units are in meV.

Σ7 NiI_2	J_{xx}	J_{yy}	J_{zz}	J_{xy}	J_{yx}	J_{xz}	J_{zx}	J_{yz}	J_{zy}
$J_{0\text{-}15}$	6.52	6.36	6.29	0.81	-0.31	0.71	-0.37	1.88	-1.52
$J_{0\text{-}17}$	-3.92	-4.94	-4.23	1.74	-0.40	-1.49	-0.57	-0.77	-0.29
$J_{16\text{-}0}$	-7.02	-8.41	-8.50	-2.1	-0.40	0.88	0.77	-0.91	-0.73
$J_{1\text{-}15}$	8.29	8.29	7.29	-1.39	1.38	0.94	-0.95	-0.15	-0.16
$J_{2\text{-}16}$	0.45	0.36	-0.14	-0.51	0.51	0.60	-0.60	-0.20	-0.19
$J_{15\text{-}16}$	-11.76	-9.51	-10.16	-1.27	1.81	0.28	0.65	1.51	1.74
$J_{15\text{-}17}$	-12.57	-11.40	-12.65	0.67	-3.01	1.87	-0.11	0.16	-1.89
$J_{15\text{-}18}$	-1.01	-2.96	-1.30	-0.20	0.87	0.32	-3.1	0.71	-1.32
$J_{16\text{-}18}$	-1.91	-1.86	-1.27	-1.27	-0.68	1.74	0.85	-0.95	-0.98
$J_{17\text{-}18}$	-7.07	-5.83	-5.97	1.52	0.11	0.73	0.07	1.19	1.00

Table S5. Exchange coupling tensors for first-nearest neighbor (J_1), second-nearest neighbor (J_2), and third-nearest neighbor (J_3), and single-ion anisotropy (SIA) in monolayer $NiBr_2$. All the units are in meV.

$NiBr_2$	J_{xx}	J_{yy}	J_{zz}	J_{xy}	J_{yx}	J_{xz}	J_{zx}	J_{yz}	J_{zy}	SIA
J_1	-7.52	-7.20	-7.36	0.00	0.00	0.00	0.00	-0.18	-0.18	
J_2	-0.11	-0.12	-0.08	0.00	0.00	0.00	0.00	0.00	0.00	0.04
J_3	3.58	3.60	3.61	0.00	0.00	0.00	0.00	0.00	0.00	

Table S6. Exchange coupling tensors for first-nearest neighbor (J_1), second-nearest neighbor (J_2), and third-nearest neighbor (J_3), and single-ion anisotropy (SIA) in monolayer NiI_2. All the units are in meV.

NiI_2	J_{xx}	J_{yy}	J_{zz}	J_{xy}	J_{yx}	J_{xz}	J_{zx}	J_{yz}	J_{zy}	SIA
J_1	-9.54	-6.03	-7.40	0.00	0.00	0.00	0.00	-1.82	-1.82	
J_2	-0.06	-0.23	0.57	-0.03	-0.03	0.00	0.00	-0.05	-0.05	0.74
J_3	6.86	7.17	7.48	0.00	0.00	0.00	0.00	-0.08	-0.08	

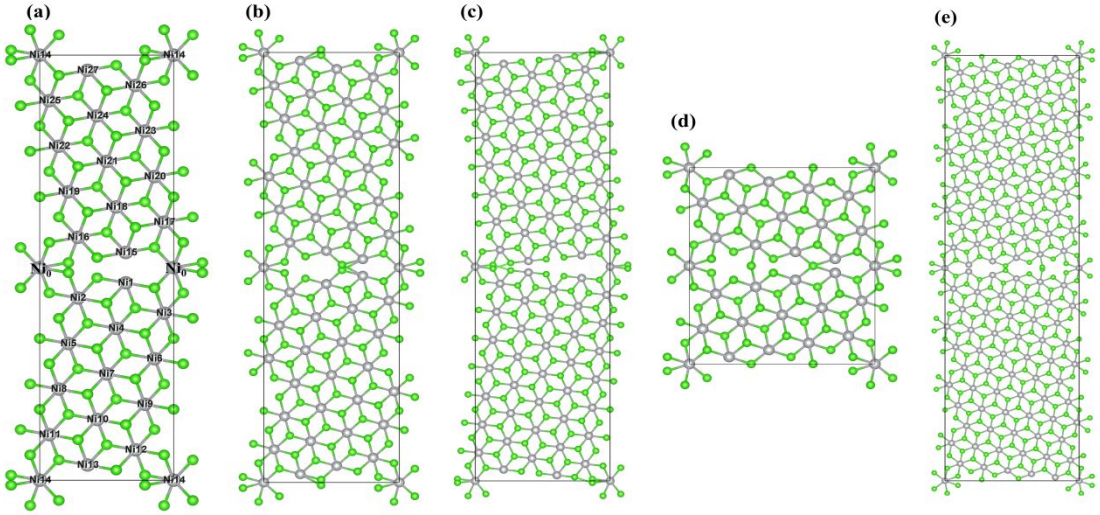

Figure S1. Constructed GB structures with (a) Σ7, (b) Σ13, (c) Σ19, (d) Σ21 and (e) Σ31. Silver and green balls denote Ni and halogen (Cl, Br and I) atoms, respectively.

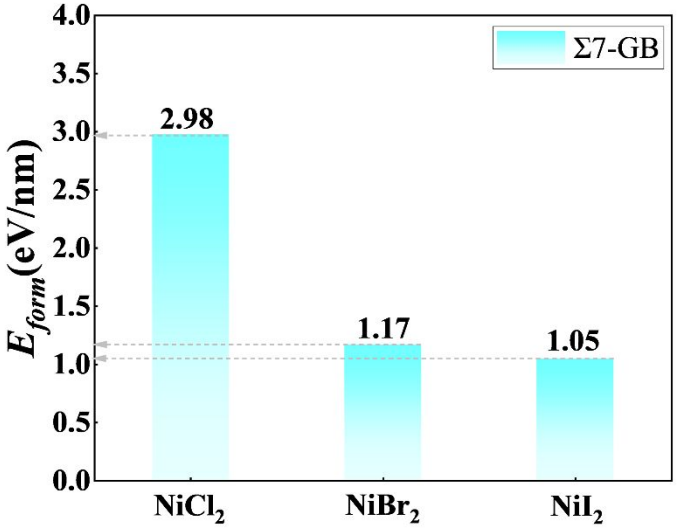

Figure S2. Comparison of Σ7 GB formation energies (E_{form}) for $NiCl_2$, $NiBr_2$, and NiI_2.

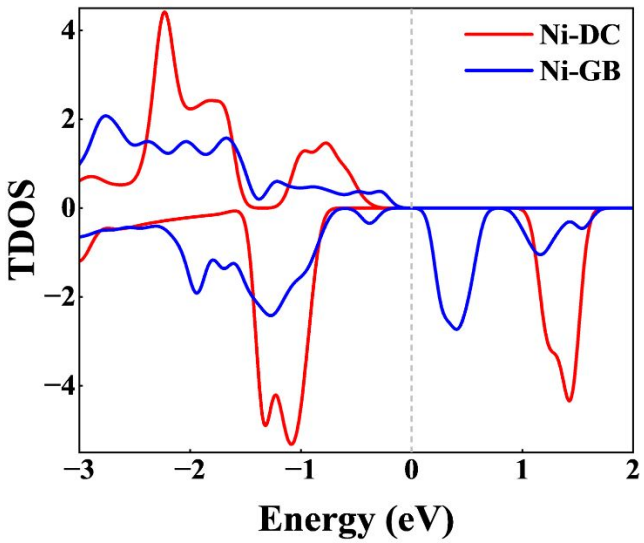

Figure S3. DOS of a Ni atom in the domain center and at the four-coordinate site in the Σ7 $NiCl_2$ GB.

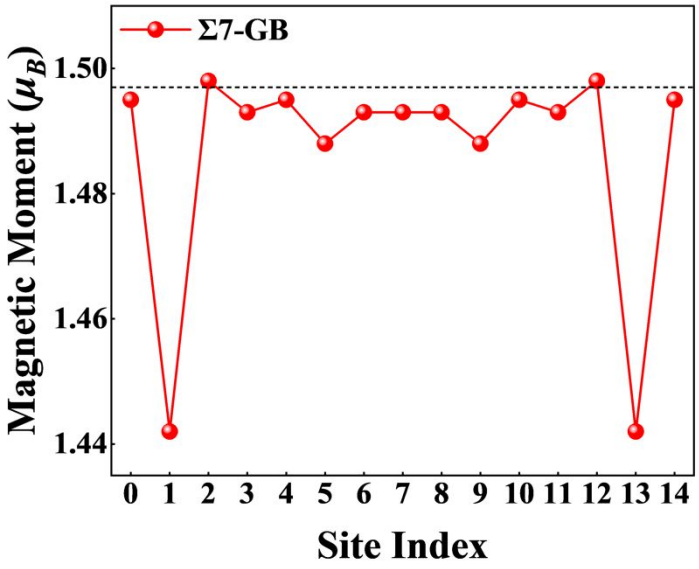

Figure S4. Magnetic moment distribution of Ni atoms at the Σ7 $NiCl_2$ GB. The black dashed line represents the magnetic moment of Ni atoms (~1.497 μ_B) in monolayer $NiCl_2$. The site index is shown in **Figure S1**.

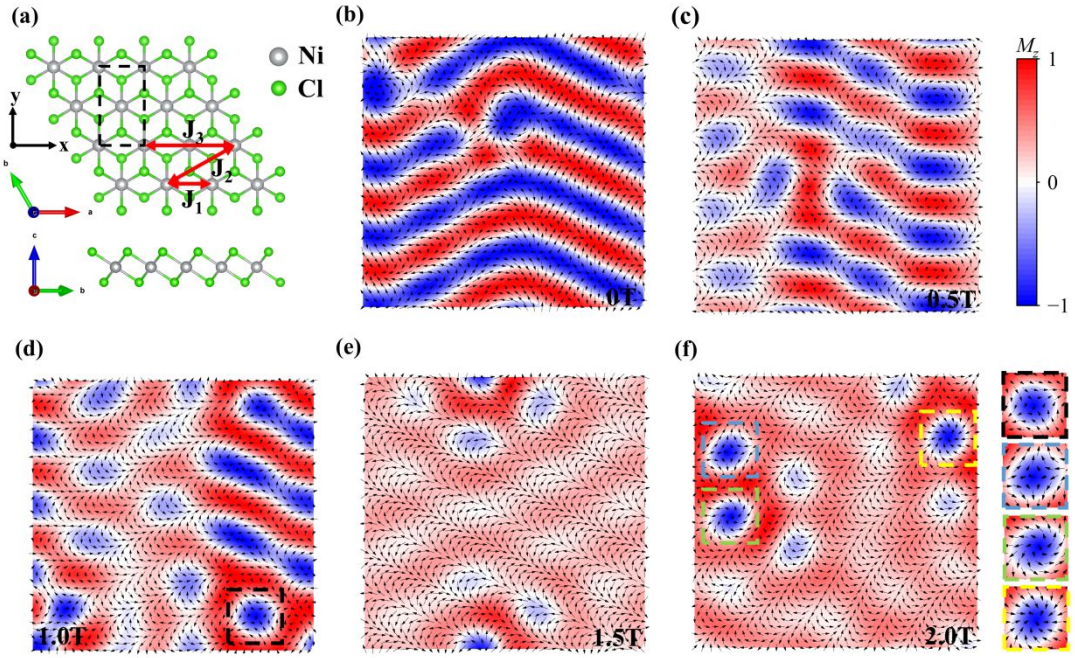

Figure S5. (a) Top and side views of monolayer $NiCl_2$. Silver and green balls denote Ni and Cl atoms, respectively. Dashed frame shows the smallest rectangle lattice in MC simulations. Spin textures of $NiCl_2$ at B_z = (b) 0T, (c) 0.5T, (d) 1.0T, (e) 1.5T, and (f) 2.0T, respectively. Black arrows denote the in-plane components of the spins, while the red-blue color map corresponds to the out-of-plane magnetization (M_z).

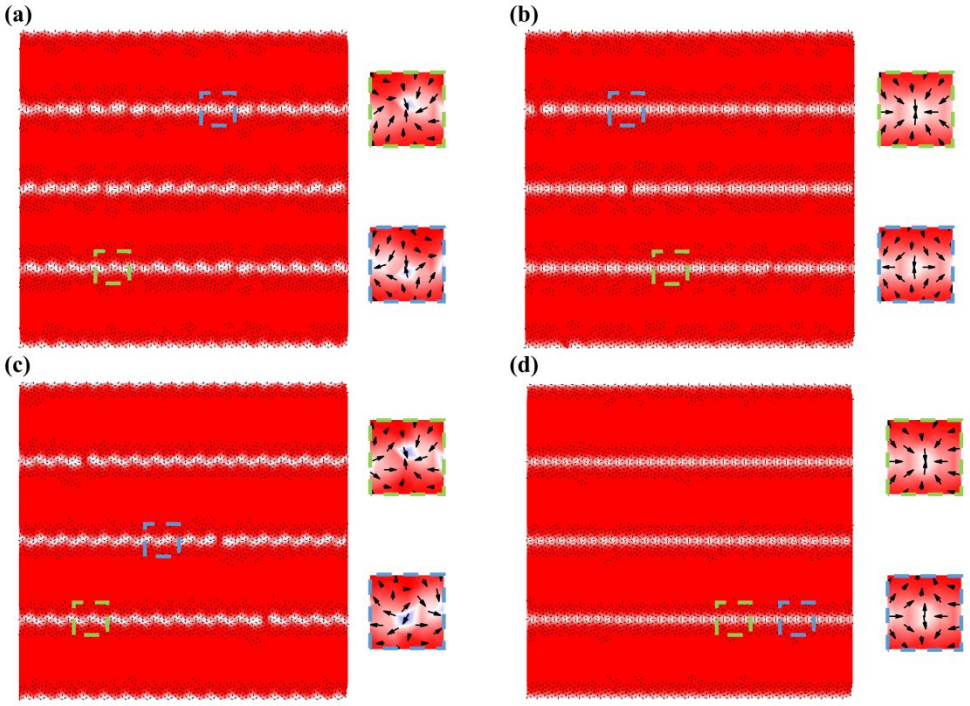

Figure S6. Spin textures of the Σ7 $NiCl_2$ at B_z = 18.0 T (a) with DM and Kitaev interactions, (b) with only Kitaev interactions, (c) with only DM interaction and (d) without DM and Kitaev interactions. Black arrows denote the in-plane components of the spins, while the red-blue color map corresponds to the out-of-plane magnetization (M_z).

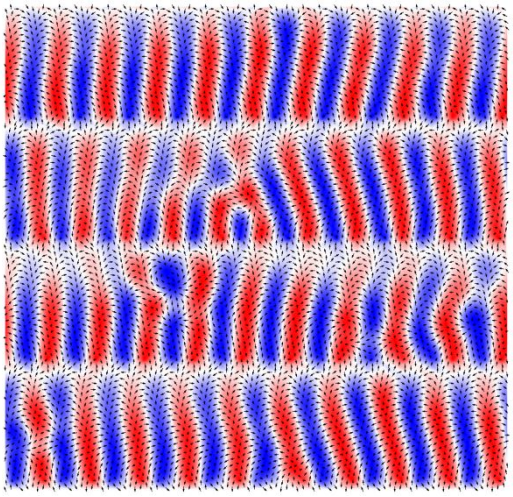

Figure S7. Spin textures of Σ7 $NiCl_2$ at B_z = 0T. The AFM interaction is artificially converted to FM at the GB. Black arrows denote the in-plane components of the spins, while the red-blue color map corresponds to the out-of-plane magnetization (M_z).

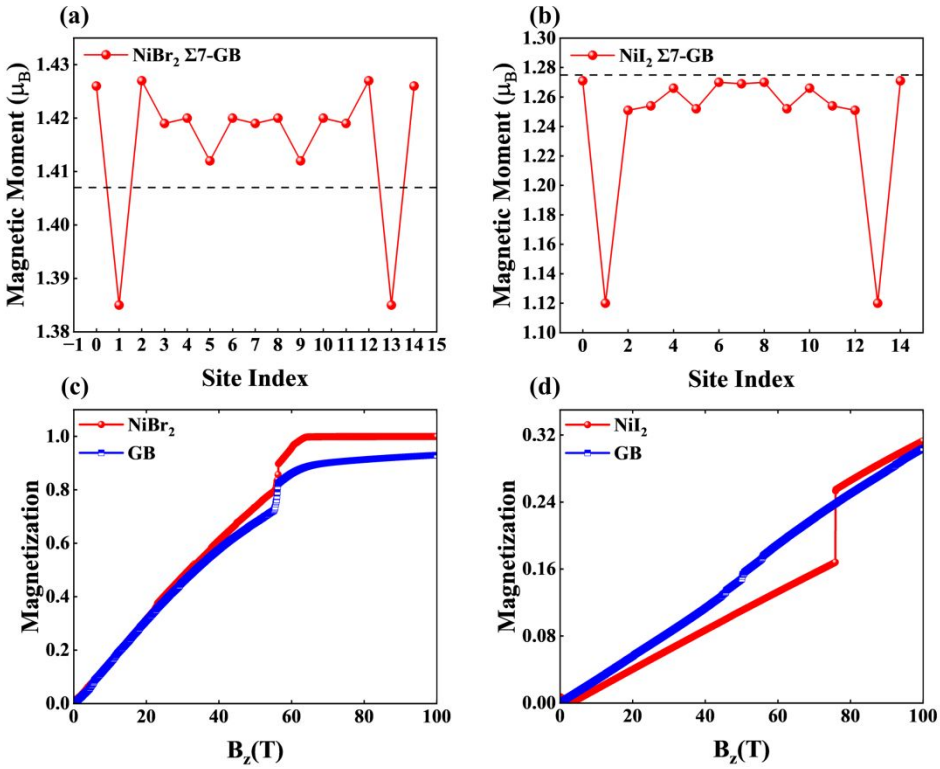

Figure S8. Magnetic moment distribution of Ni atoms at the (a) Σ7 $NiBr_2$ and (b) Σ7 NiI_2. The black dashed line indicates the magnetic moment of Ni atoms in monolayer. Initial magnetization curves for (c) $NiBr_2$ and (d) NiI_2.

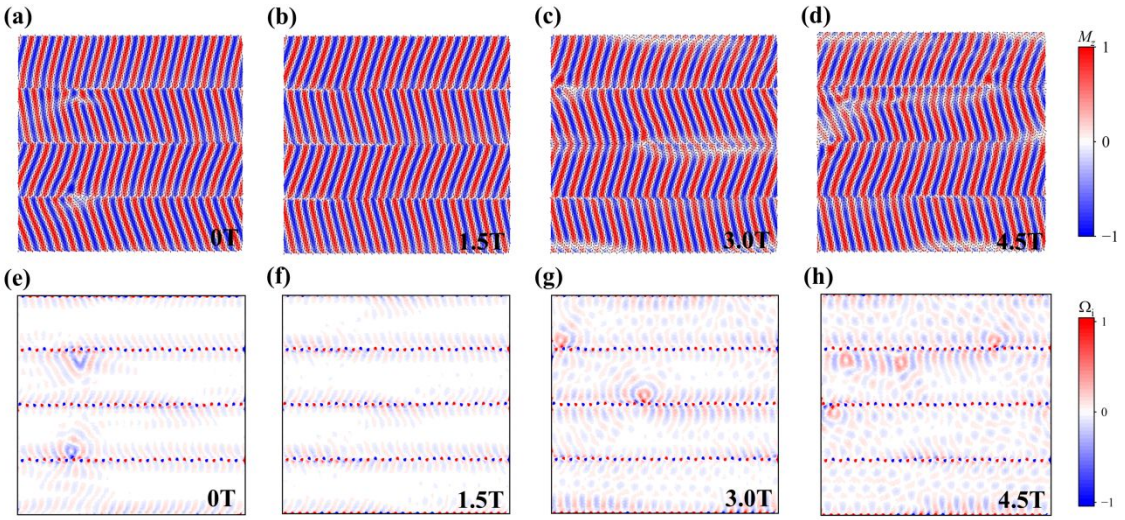

Figure S9. The spin textures of Σ7 $NiBr_2$ at B_z = (a) 0T, (b) 1.5T, (c) 3.0T, and (d) 4.5T, respectively. Panels (e)-(h) show the spin scalar chirality (Ω_i) at corresponding magnetic fields.

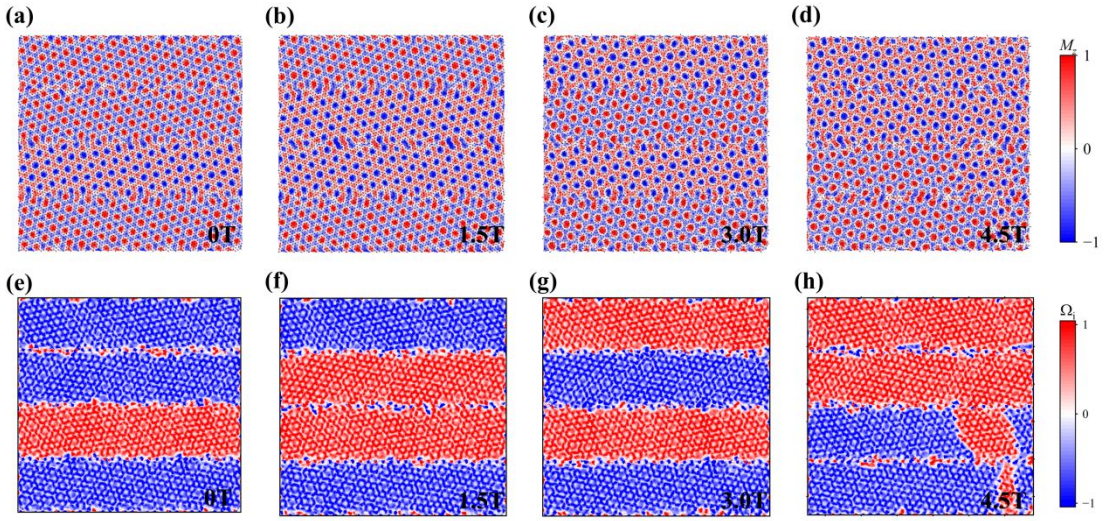

Figure S10. The spin textures of Σ7 NiI_2 at B_z = (a) 0T, (b) 1.5T, (c) 3.0T, and (d) 4.5T, respectively. Panels (e)-(h) show the spin scalar chirality (Ω_i) at corresponding magnetic fields.

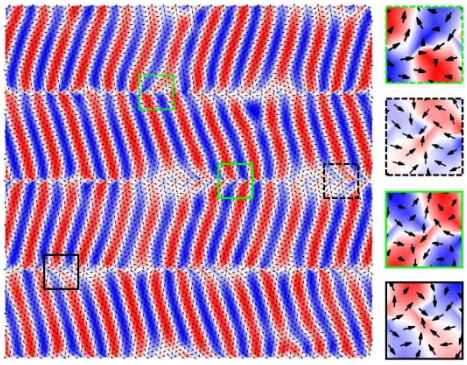

Figure 11. Spin texture for Σ7 NiBr2 at B_z=0 when artificially change the initial random Monte Carlo seed.

References:

(1) Kresse, G.; Furthmüller, J. Efficiency of ab-initio total energy calculations for metals and semiconductors using a plane-wave basis set. *Comput*. *Mater*. *Sci*. **1996**, 6, 15-50.

(2) Perdew, J. P.; Burke, K.; Ernzerhof, M. Generalized gradient approximation made simple. *Phys*. *Rev*. *Lett*. **1996**, 77, 3865.

(3) Amoroso, D.; Barone, P.; Picozzi, S. Spontaneous skyrmionic lattice from anisotropic symmetric exchange in a Ni-halide monolayer. *Nat*. *Commun*. **2020**, 11, 5784.

(4) Dudarev, S. L.; Botton, G. A.; Savrasov, S. Y.; Humphreys, C. J.; Sutton, A. P. Electron-energy-loss spectra and the structural stability of nickel oxide: An LSDA+U study. *Phys*. *Rev*. *B* **1998**, 57, 1505.

(5) Martyna, G. J.; Tobias, D. J.; Klein, M. L. Constant pressure molecular dynamics algorithms. *J*. *Chem*. *Phys*. **1994**, 101, 4177.

(6) Kosov, D. S.; Gelin, M. F.; Vdovin, A. I. Calculations of canonical averages from the grand canonical ensemble. *Phys*. *Rev*. *E* **2008**, 77, 021120.

(7) Xiang, H. J.; Lee, C.; Koo, H. J.; Gong, X. G.; Whangbo, M. H. Magnetic properties and energy-mapping analysis. *Dalton*. *Trans*. **2013**, 42, 823.

(8) Šabani, D.; Bacaksiz, C.; Miloševic, M. V. Ab initio method-ology for magnetic exchange parameters: Generic four-state energy mapping onto a Heisenberg spin Hamiltonian. *Phys*. *Rev*. *B* **2020**, 102, 014457.

(9) Evans, R. F.; Fan, W. J.; Chureemart, P.; Ostler, T. A.; Ellis, M. O.; Chantrell, R. W. Atomistic spin model simulations of magnetic nanomaterials. *J*. *Phys*: *Condens*. *Matter*. **2014**, 26, 103202.

(10) Berg, B.; Lüscher, M. Definition and statistical distributions of a topological number in the lattice O(3) σ-model. *Nucl*. *Phys*. *B*. **1981**, 190, 412-424.